The 2013 World Congress on
Advances in Structural Engineering and Mechanics (ASEM13)
Jeju, Korea, September 8-12, 2013

Evaluation of bulk properties of structural materials from small-scale mechanical tests

*Tae-Hong Ahn[1)], Chansun Shin[2)], Heung Nam Han[3)] and Junhyun Kwon[4)]

[1), 4)] *Nuclear Material Technology Division, KAERI, Daejeon 305-353, Korea*
[2)] *Department of Materials Science and Engineering, Myongji University, Yongin 449-728, Korea*
[3)] *Department of Materials Science and Engineering, Seoul National University, Seoul 151-744, Korea*
[1)] *thahn@kaeri.re.kr*

ABSTRACT

The response of structural materials to nanoindentation and micropillar compression test were investigated. Nanoindentation and microstructural studies of automotive and structural steels were carried out in order to provide the micromechanical insight into the several stress-induced physical phenomena which play important roles in the deformation of steels. The mechanism of martensitic transformation of austenite, yield drop and strain aging effect of ferrite were explained in microstructural and crystallographic viewpoint. It is also reported that the micropillar compression test can be an outstanding testing technique for measuring bulk properties of materials when macro-scale measuring methods are limited due to the special conditions of materials (e.g., nuclear reactor materials). The sample size-dependence of yield stress for 3C-SiC was investigated by micropillar compression test, and the transition size above which size-independent strengths can be measured was also evaluated.

1. INTRODUCTION

Recently, small-scale mechanical testing techniques (e.g., nanoindentation, micropillar compression, etc.) have been widely used to probe the mechanical properties of materials for a wide range of academic and engineering applications, owing to their favorable advantages that these techniques can evaluate not only the micro-scale properties but also the macro-scale properties by measuring only small volumes of a material. In nanoindentation, the most commonly measured material properties are hardness and elastic modulus. However, besides these properties, nanoindentation gives the real-time behaviors of a material against the applied force as well, which is generally represented as a form of a load-displacement curve. This real-time depth-sensing method enables to detect many discrete physical events that occur during deformation, such as incipient plasticity (Bei 2008), phase transformations (Ahn 2010) or mechanically-induced twinning (Misra 2010). These dynamic events are usually presented as sudden displacement change on the load-displacement curve,

termed as a “pop-in”.

Micropillar compression test has attracted considerable interest on account of demands for the mechanical test on the downscaled devices. However, the sample size effects on material strength gave rise to complication in extracting bulk properties from the test. Size-dependent strength is controlled by dislocation source limitation when the specimen size is below hundreds of nanometers (Uchic 2004), whereas for larger samples it is controlled by defects in the pillar such as grain boundaries, precipitations, or impurities (Kiener 2011).

The present article consists of two main parts of experimental studies of small-scale mechanical testing. In the first part, experimental results of nanoindentation and microstructural studies of automotive and structural steels will be reported. By comparing them to the bulk-scale mechanical behaviors, the micromechanical insight into the several stress-induced physical phenomena which play important roles in the deformation of steels will be provided. In the second part, it will be reported that the micropillar compression test can be an outstanding testing technique for measuring bulk properties of materials when macro-scale measuring methods are limited due to the special conditions of materials (e.g., nuclear reactor materials). The sample size-dependence of yield stress for a nuclear material was investigated by micropillar compression test, and the transition size above which size-independent strengths can be measured was also evaluated.

2. EXPERIMENTAL

For nanoindentation studies, a multiphase transformation-induced plasticity (TRIP) steel (Fe-0.08C-0.5Si-1Al-7Mn (wt.%)) and a commercial ferritic steel were prepared. EBSD was used for phase identification and nanoindentation tests were performed under load control condition at a constant loading rate using a Berkovich type indenter. Guided by the EBSD and SPM images, selective indentations on desired individual grains could be made. Cross section TEM analysis of the indented austenite grain was performed to confirm strain-induced martensite directly under the indent with a sample prepared by focused ion beam (FIB) milling. For a ferritic steel, nanoindentation and tensile tests were performed on annealed specimens, prestrained specimens, and specimens aged for various times after prestraining in order to investigate the effect of dislocation locking by interstitial atoms on nanoindentation pop-in.

A plate of commercially available CVD 3C-SiC (Morgan Advanced Ceramics Inc., CVD Materials) was used for micropillar compression test. The SiC micropillars were fabricated from a polycrystalline 3C-SiC plate using lithography, plasma etching and finally annular milling in an FIB machine to produce a smooth surface. The diameters of the pillars ranged from 4.7 down to 0.65 μm. The aspect ratio (pillar height/diameter) was maintained at between 2 and 4 to avoid a triaxial stress state and buckling for a low- and high-aspect ratio, respectively. The micropillars were compressed using a nanoindenter equipped with a flat-ended conical diamond punch 15 μm in diameter. The tests were performed at a nominally constant displacement rate of 5 nm/s.

3. RESULTS AND DISCUSSION

3.1 Nanoindentation behavior of metastable retained austenite (Ahn 2010)

Fig. 1 (a) shows a typical EBSD phase map of the TRIP steel samples, showing well-defined FCC austenite and BCC ferrite grains with a mean grain size of approximately 0.7 μm. Fig. 2 gives the load-displacement curve (black symbols) obtained by nanoindentation of one of retained austenite grains which is circled in Fig. 1 (a). Three pop-ins were measured during loading segment of the indentation. Generally, it is known that on carefully polished metal surfaces the deformation before the first pop-in has been shown to be perfectly elastic (Bei 2008). Assuming that the indenter tip is spherical at shallow depths, the measured curve before the first pop-in can be compared with the Hertzian elastic contact solution (Johnson 1985). According to Gouldstone *et al.* (2000), for an indenter tip radius of 200nm and centerline-to-face angle of 65.3^{o}, the depth at which the tip geometry transitions from spherical to Berkovich is approximately 36.5nm. Therefore, we assume here that at depths below about 20nm in Fig. 2, where the first pop-in occurs, indentation occurs with a spherical tip.

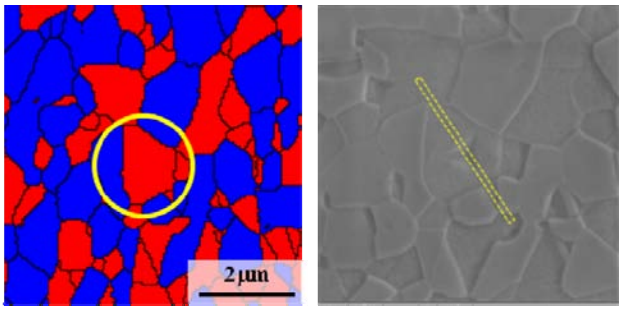

(a) (b)

Fig. 1 (a) An EBSD phase map (Red: FCC, Blue: BCC). (b) Dotted yellow lines on SEM image showing schematically where FIB milling was used to cut out a cross-section through the indent for TEM analysis

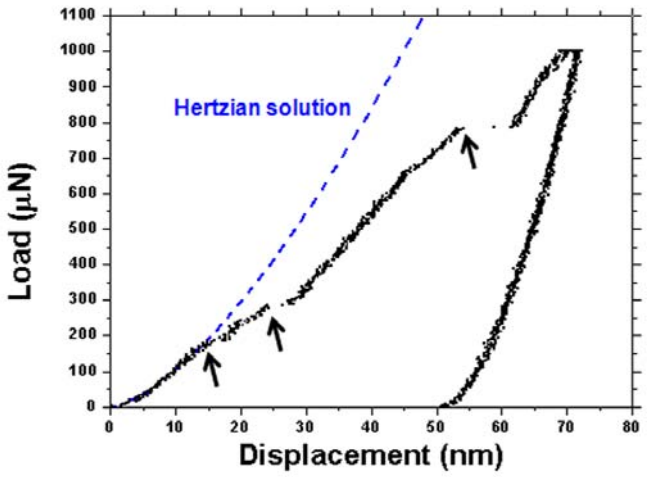

Fig. 2 A load-displacement curve of the indented austenite grain

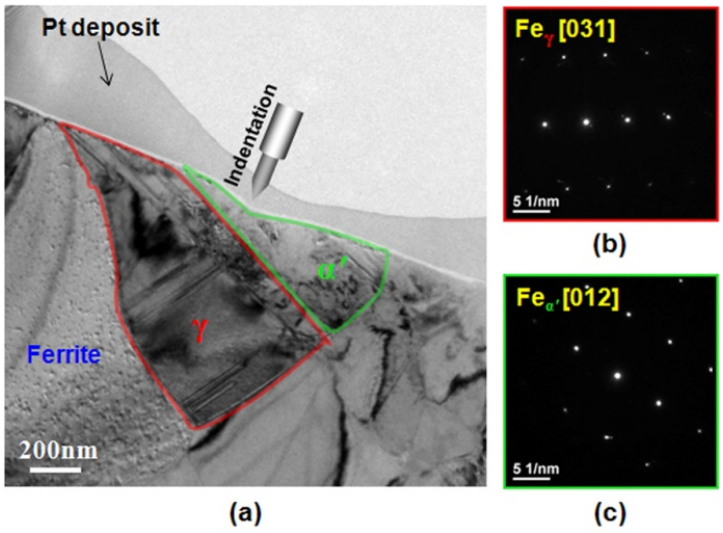

Fig. 3 Cross-section TEM observations of the indented grain. (a) A plane-view image, (b) and (c) diffraction pattern of austenite and martensite region, respectively

The theoretical Hertzian elastic behavior during indentation was calculated using this effective modulus of austenite and the isotropic elastic constants of the diamond tip. The results are shown by the blue dashed line in Fig. 2. Before the first pop-in, the theoretical curve matches the experimental loading curve well indicating that the region below the first pop-in is elastic while that above it is plastic. Therefore, it is thought that the first pop-in which occurs at very beginning part of the indentation is originated from elastic-to-plastic deformation transition, which can often be found from nanoindentation inside a grain of crystalline materials (Bei 2008).

After the first pop-in, there are two more pop-ins that begin at depths of ~25 and 50nm, as shown in Fig. 2. It is possible that these are related to the strain-induced martensitic transformation from metastable austenite. In order to investigate the presence of martensite under the indentation, the cross-section of a sample indented to a depth of ~70nm, which is slightly beyond the third pop-in, was prepared (Fig. 1(b)) and examined by TEM. As shown in the bright field TEM image in Fig. 3, there is an obvious indent on the surface and two regions with distinctly different morphologies inside the grain adjacent to the indent. From an analysis of the diffraction patterns for these two regions, the region closest to the indent was determined to be transformed martensite while the rest of the parent grain remained as austenite with some stacking faults. This microstructural observation strongly suggests that one or both of the pop-ins on the load-displacement curve corresponds to the onset of a strain-induced martensitic transformation.

But since martensite is much harder than austenite, and the lattice parameter of martensite is larger than that of austenite, the appearance of martensite during deformation must increase the strain hardening rate. Therefore, the softening implied by the pop-ins must be explained. In this paper, an attempt is made to understand the pop-in behavior using the concept of favorable variant selection in the strain-induced martensite during nanoindentation. It is well known that transformed martensite usually

has an orientation relationship with its parent austenite phase, referred to as the Kurdjumov–Sachs (K–S) relation (Kurdjumov 1930). Each of the 24 K–S variants has one compressive axis and two tensile axes for the martensitic transformation, as shown in Fig. 4, which is called the Bain distortion. It is natural that a variant whose compressive axis of the Bain distortion is nearly parallel to the indentation direction should have a higher probability of selection. Moreover, since the martensitic transformation is a nucleation-controlled process and its speed is quite fast, the indenter tip must react rapidly as the strain-induced phase transformation occurs in order to maintain a constant loading rate in load control, which leads to a pop-in.

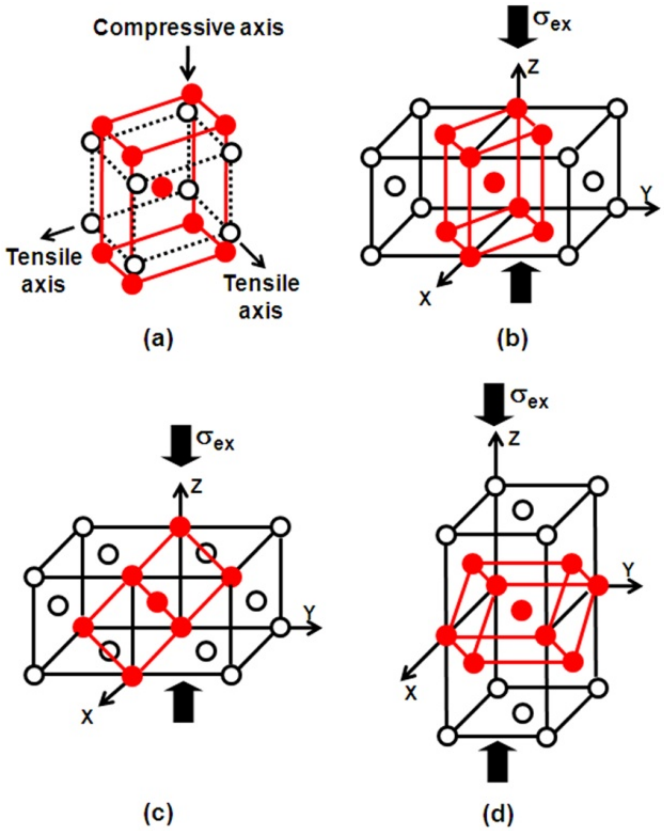

Fig. 4 Schematic diagrams for Bain distortion:
(a) Movement of crystal lattices for FCC-to-BCT transformation;
(b), (c) and (d) Three different Bain variants depending on the direction of the compression axis

3.2 Relationship between yield drop and nanoindentation pop-in (Ahn 2012)

Fig. 5 presents the stress-strain curves obtained from uniaxial tensile tests of a ferritic steel. For the fully annealed specimen, a sharp yield point is clearly observed. After the initial elastic portion, a significant yield drop occurred at the upper yield point, followed first by Lüders strain propagation and then uniform elongation accompanied by work hardening. In the case of specimens that were deformed to 6% nominal strain,

unloaded, and then reloaded, their behavior depended on the strain aging time. When reloaded right after unloading, the material did not show a clear yield drop, as shown in Fig. 5(a). In contrast, a sharp yield point was observed when the specimen was reloaded after 30 hours of strain aging, as shown in Fig. 5(b). These results are typical of yield point phenomena seen in steels.

Interestingly, similar behaviors were also observed in the nanoindentation tests. Figs 6(a-d) show the load-displacement curves for nanoindentations performed before, right after, 30 hours after, and 3 weeks after 6% pre-strain. Before the pre-strain (i.e., annealed state), large and obvious pop-ins were observed on the loading curves for most of the indentations at quite high loads (100~700μN), as shown in Fig. 6(a). Before the first pop-ins, the experimental loading curves match the theoretical curve well, indicating elastic response before pop-in. The maximum shear stress underneath the indenter τ_m at pop-in ($\tau_{pop\text{-}in}$) for the annealed specimen was determined to be in the range 3.3~5.3GPa, which corresponds to $G/25$~$G/15$ where G, the shear modulus of ferrite at room temperature, is 80.7GPa. These values of $\tau_{pop\text{-}in}$ are within the range of values for the theoretical strength (τ_{th}) of a crystalline material, indicating that the pop-ins in the annealed specimen are likely the result of dislocation nucleation.

Fig. 6(b) shows representative load-displacement curves for nanoindentation tests performed right after the pre-strain. No distinct pop-in was observed on any of these curves. Instead, most of the curves showed only a slight change of slope without a clear pop-in to mark the onset of plasticity. The transition loads were relatively low, less than 100μN, indicating elastic-plastic deformation practically right from the start of indentation in the pre-strained specimen.

Figs. 6(c) and (d) show the nanoindentation load-displacement curves obtained 30 hours and 3 weeks after the pre-strain, respectively. In both cases, distinct pop-ins reappeared for some of the indentations, while they were never observed when the specimen was indented right after the pre-strain. Moreover, as shown in Figs. 6(b-d), the pop-in loads increased with increasing strain aging time.

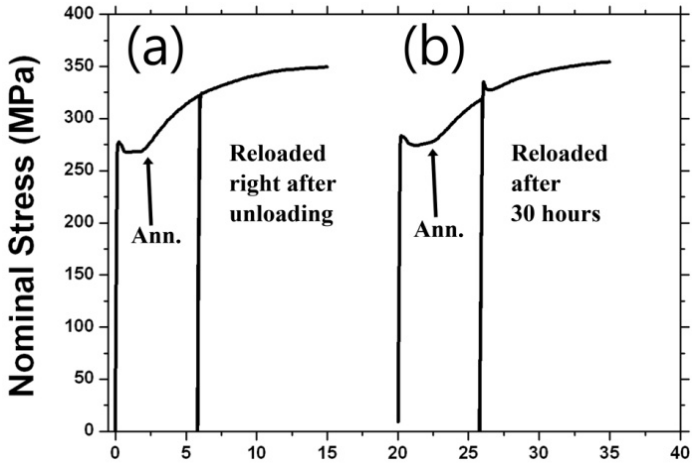

Fig. 5 Uniaxial tensile stress-strain curves for the annealed specimen (arrows) with those obtained after (a) loading to 6% strain, unloading and then immediately reloading and (b) loading to 6% strain, unloading, strain aging for 30 hours, and then reloading. The curves in (b) are offset from the origin for clarity of presentation.

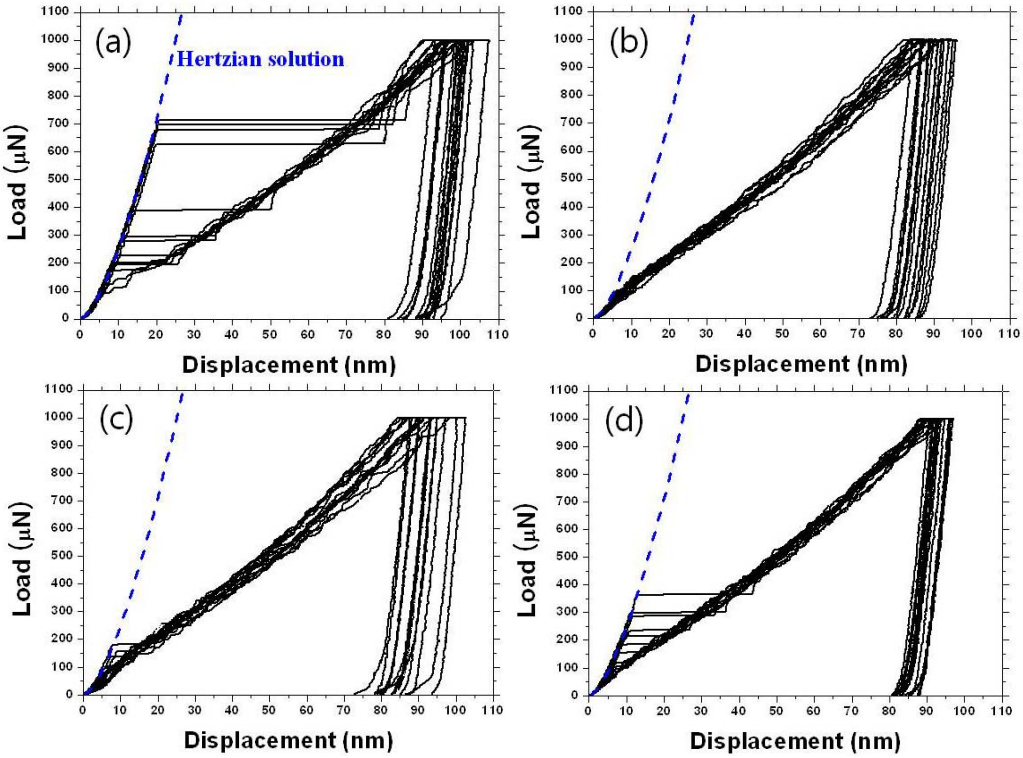

Fig. 6 Nanoindentation load-displacement curves obtained (a) before, (a) right after, (c) 30 hours after and (d) 3 weeks after 6% tensile pre-strain

For the pop-in loads shown in Fig. 6, the maximum shear stresses under the indenter ($\tau_{pop\text{-}in}$) were calculated as discussed earlier. Fig. 7 shows these calculated pop-in stresses (average values ± 1 standard deviation) for the annealed, pre-strained, and strain-aged conditions. The annealed specimen pops-in at the theoretical strength, consistent with the notion that plastic deformation of dislocation-free volumes requires nucleation of dislocations. After 6% tensile pre-strain, however, the pop-ins disappear, indicating that, if there are enough mobile dislocations in the stressed volume, plastic deformation can occur by movement of these pre-existing dislocations at very low loads (essentially right from the start of deformation) rather than by the nucleation of new dislocations at very high stresses.

What has not been investigated until now is the effect of interstitial solute atoms on pop-in behavior. At the macroscopic scales of tensile tests, the origin of the sharp yield point is known to be dislocation locking by interstitial solute atoms, the so-called Cottrell atmosphere (Cottrell 1953). In order to free a dislocation from this atmosphere, additional stress over that normally required for dislocation movement is needed resulting in a sharp yield drop after the dislocations break free and multiply. We find here that an analogous situation exists in the case of nanoindentation where the softening is manifested as a pop-in. Immediately after the 6% pre-strain, the steel has a high density of new dislocations which are relatively mobile because they have not yet been pinned by the solute atoms. Therefore, both the sharp yield points (Fig. 5(a)) and the distinct pop-ins (Fig. 6(a)) disappear. However, when the solute atoms diffuse to the

dislocations as the aging time increases, they tend to anchor the dislocations again, which results in a recovery of the yield point phenomenon (Fig. 5(b)). When a nanoindentation is made near a location where the dislocations are pinned, a higher stress is needed to unlock them. This causes a reappearance of the pop-in (clear elastic-to-plastic transition). These nanoindentation and tensile test results strongly suggest that the pop-in behavior in ferrite is closely related to its yield point phenomenon.

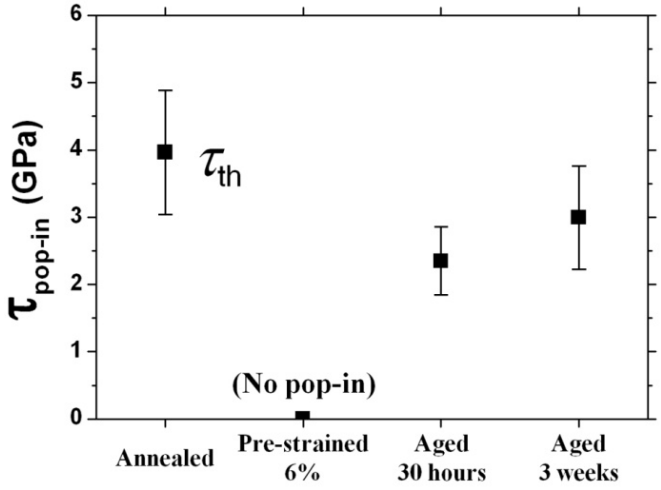

Fig. 7 Nanoindentation pop-in stresses before, right after, 30 hours after, and 3 weeks after the 6% tensile strain

3.3 Micropillar tests of CVD 3C-SiC (Shin 2012)

Fig. 8(a) shows a typical engineering stress-strain curve. After the initial elastic loading, a rapid burst in the indenter displacement occurred and the indenter overshot to maximum displacement, which corresponds to the height of each pillar. This rapid burst indicates a brittle fracture, and the sample could not be unloaded before it failed. The compressive elastic modulus was evaluated to be ~450 GPa from the elastic loading part, which is consistent with the value of ~465 GPa reported in the literature for a dense and high-purity CVD SiC. The compressive strengths, i.e., the maximum stress at which a catastrophic failure occurred, are plotted in Fig. 8(b) as a function of diameter. The fracture strength and its scatter increased with a decrease in diameter. The compressive strengths measured from the pillars, the surfaces of which were smoothed by FIB, e.g., Figs. 9(e) and (f), are plotted as red diamonds in Fig. 8(b). The measured strengths were in good agreement with those measured from the pillars without the surface smoothing process. This result indicates that the vertical striations on the surface of larger pillars had a negligible effect on the measured fracture strength and were not the crack initiation sites. The potential sites for crack initiation are the grain boundaries of CVD SiC because the grain boundary is known to be the weak point for crack initiation (Zhao 2011). The observed dependence of the compressive

strength on the pillar diameter can be accounted for the fact that the strength at the inner weakest flaw determines the overall strength of brittle ceramic materials. In our work, a decrease in pillar size led to a reduced probability of finding the weakest flaws, i.e., grain boundaries, and hence an increase in the compressive strength.

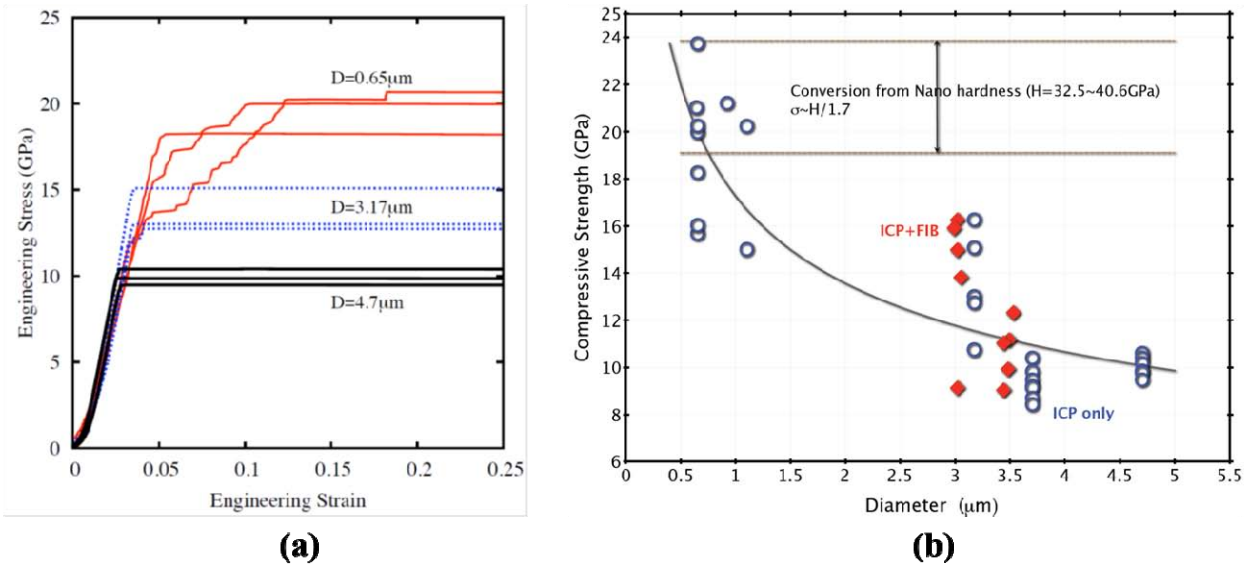

Fig. 8 (a) Engineering stress-strain curves for micropillars and
(b) plot of compressive strength as a function of the micropillar diameter

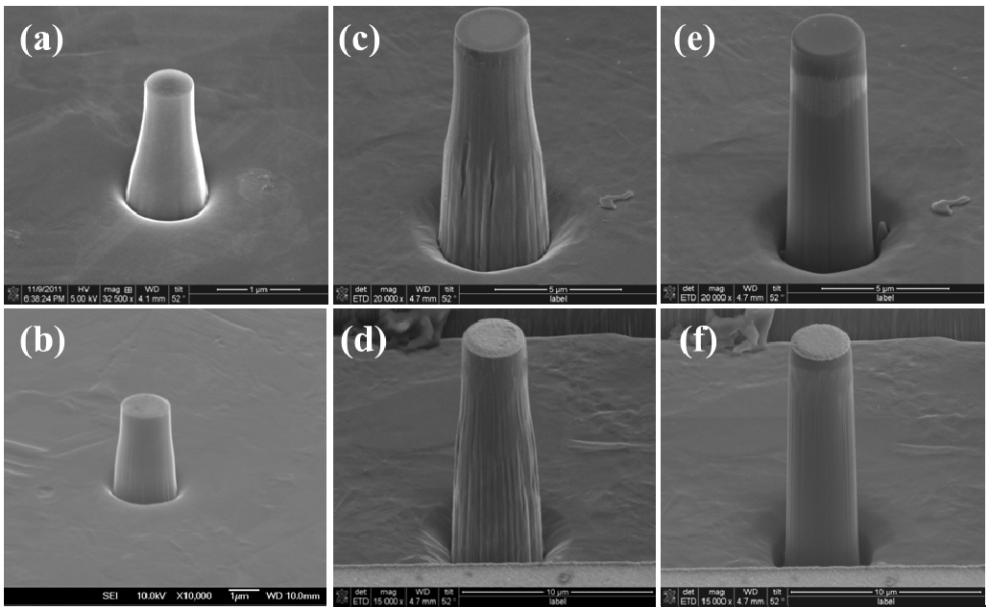

Fig. 9 SEM micrographs of SiC micropillars with a nominal diameter of (a) 0.65, (b) 1.1, (c) 3.17, (d) 3.70 μm fabricated by ICP etching, and (e) 3.17, and (f) 3.70 μm, whose vertical striations on the surface were removed by FIB milling. All images were taken at a ~50° stage tilt

The pillars with a diameter larger than 1 lm failed catastrophically with a negligible amount of plastic flow. The micropillars with a diameter of 0.65 μm, however, displayed a discrete transition from elastic to plastic flow. Several discrete strain bursts were observed at the transition regime, as the tests were conducted under a load control. The pillar could be deformed by almost 12% before fracturing. Fig. 10 (a) shows such a plastically deformed pillar. The upper portion of the pillar was plastically deformed, and slip bands can be observed on the surface of the compressed pillar. Fig. 10(b) shows a TEM micrograph of the cross-sectional TEM specimen of the plastically deformed pillar shown in Fig. 10(a), prepared by a lift-out technique in FIB. A slip initiated from the left-top corner of the pillar and propagated through the pillar producing steps on the right surface of the pillar. A slip was found to occur on the {111} plane from a diffraction pattern, which corresponds to a <110>{111} slip system of an fcc zinc-blende structured 3C-SiC. A close-up of slip bands in the left-top part of the pillar showed that dislocation movement in the slip bands has sheared the pre-existing stacking faults. The critical resolved shear stress of 3C-SiC could be experimentally determined and was evaluated as 4.9–7.3 GPa.

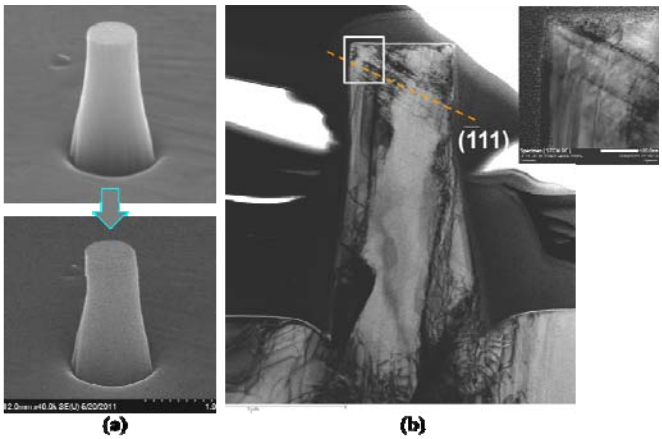

Fig. 10 (a) SEM micrographs of plastically deformed SiC micropillar,
(b) TEM micrograph of the cross-sectional TEM specimen prepared from the micropillar in (a)

4. CONCLUSIONS

(1) The nanoindentation load-displacement curve for austenite revealed two types of pop-in events on the loading segment. The first type was attributed to the elastic-to-plastic transition of austenite based on a Hertzian analysis of the elastic portion of the load-displacement curve. A second type of pop-in can be described as resulting from geometrical softening due to the selection of a favorable martensite variant based on the mechanical interaction energy between the externally applied stress and lattice deformation during nanoindentation.
(2) The relationship between pop-in behavior during nanoindentation and yield point

phenomena in tensile tests was investigated by comparing the mechanical responses of pre-strained and strain-aged ferritic steel. The pop-ins observed on the load-displacement curves of the annealed specimens (i.e., before tensile pre-straining), were attributed to dislocation nucleation based on Hertzian analyses. Their disappearance right after pre-straining and reappearance after strain aging, similar to the disappearance and reappearance of yield drops in tensile tests, strongly suggest that nanoindentation pop-ins in ferritic steel are closely related to their yield points. Both phenomena are influenced by dislocation locking by solutes (Cottrell atmospheres).

(3) SiC micropillars were fabricated with a diameter ranging from 0.65 to 4.7 lm from a CVD 3C-SiC polycrystalline plate using lithography and ICP etching techniques. The compressive strength displayed a size dependency in terms of the pillar diameter. This can be attributed to the flaw sensitivity of brittle materials, and the flaws were grain boundaries in this case. The microcompression tests of the SiC micropillars showed a brittle fracture at a certain compressive strength at room temperature, but the micropillars with a diameter of 0.65 lm showed a plastic flow before a fracture at room temperature. Through a cross-sectional TEM observation it was found that the slip occurred on the {111} slip planes, and the measured stress-strain curves and the orientation relation observed in the TEM gave the critical resolved shear stress values of 4.9–7.3 GPa.

REFERENCES

Ahn, T.-H., Oh, C.-S., Kim, D.H., Oh, K.H., Bei, H., George, E.P. and Han, H.N. (2010), “Investigation of strain-induced martensitic transformation in metastable austenite using nanoindentation”, *Scripta Mater.,* Vol. **63**, 540-543.

Ahn, T.-H., Oh, C.-S., Lee, K., George, E.P. and Han, H.N. (2012), “Relationship between yield point phenomena and the Nanoindentation pop-in behavior of steel”, *J. Mater. Res.*, Vol. **27**, 39-44.

Bei, H., Gad, Y.F., Shim, S., George, E.P. and Pharr, G.M. (2008), “Strength differences arising from homogeneous versus heterogeneous dislocation nucleation”, *Phys. Rev. B*, Vol. **77**, 060103(R).

Cottrell, A.H. (1953), “*Dislocations and Plastic Flow in Crystals*”, Oxford Univ. Press, London, England.

Gouldstone, A., Koh, H.-J., Zeng, K.-Y., Giannakopoulos, A.E. and Suresh, S. (2000), “Discrete and continuous deformation during nanoindentation of thin films” *Acta Mater.*, Vol. **48**, 2277-2295.

Johnson, K.L. (1985), *Contact Mechanics*, Cambridge University Press, Cambridge, England.

Kiener, D., Hosemann, P., Maloy, S.A. and Minor, A.M. (2011), “In situ nanocompression testing of irradiated copper”, *Nature Mater.*, Vol. **10**, 608-613.

Kurdjumov, G. and Sachs, G. (1930), “Über den mechanismus der stahlhärtung”, *Z. Phys.*, Vol. 64, 325-343.

Misra, R.D.K., Zhang, Z., Jia, Z., Somani, M.C. and Karjalainen, L.P. (2010), “Probing deformation processes in near-defect free volume in high strength–high ductility

nanograined/ultrafine-grained (NG/UFG) metastable austenitic stainless steels", *Scripta Mater.*, Vol. **63**, 1057-1060.
Shin, C., Jin, H.-H., Kim, W.-J., and Park, J.-Y. (2012), "Mechanical properties and deformation of cubic silicon carbide micropillars in compression at room temperature", *J. Am. Ceram. Soc.*, Vol. **95**, 2944-2950.
Uchic, M.D., Dimiduk, D.M., Florando, J.N. and Nix, W.D. (2004), "Sample dimensions influence strength and crystal plasticity. *Science*, Vol. **305**, 986-989.
Zhao, X., Langford, R.M., Shapiro, I.P. and Xiao, P. (2011), "Onset plastic deformation and cracking behavior of silicon carbide under contact load at room temperature", *J. Am. Ceram. Soc.*, Vol. **94**, 3509-3514.